# ON THE ANALYSIS OF ON-BOARD SENSING AND OFF-BOARD SENSING THROUGH WIRELESS COMMUNICATION FOR UAV PATH PLANNING IN WIND FIELDS

by

MURILO AUGUSTO PINHEIRO

Presented to the Faculty of the Graduate School of
The University of Texas at Arlington in Partial Fulfillment
of the Requirements
for the Degree of

MASTER OF SCIENCE IN ELECTRICAL ENGINEERING

THE UNIVERSITY OF TEXAS AT ARLINGTON
May 2019

Copyright © by MURILO AUGUSTO PINHEIRO 2019

All Rights Reserved

In the first place, I would like to express my gratitude for the opportunity to study at The University of Texas at Arlington and for all the support my parents have given and will always give me. I am also thankful to all my family members that although are far away, they always have hoped for my success. In addition, I would like to say a very special thank you to Sohail and Shamsa that introduced me to this university and for all their love and guidance. Thank you to Leena for the patience throughout this journey and for always motivating me to become a better person. Finally, I thank all the people and friends that were involved in this journey and that contributed in pursuing my goals.

ACKNOWLEDGEMENTS

I would like to thank my supervising professor Dr. Yan Wan, for giving me the opportunity to work under her supervision. I am grateful for all the guidance, support and patience given throughout my studies. I also thank Dr. Dogan for the opportunity to have him as my co-advisor. I am thankful to Dr. Schizas for reserving some time of his busy schedule to serve in my defense. Finally, I appreciate the support from the National Science Foundation under grant numbers 1724248, 1730675 and 1714519.

April 18, 2019

# ABSTRACT

## ON THE ANALYSIS OF ON-BOARD SENSING AND OFF-BOARD SENSING THROUGH WIRELESS COMMUNICATION FOR UAV PATH PLANNING IN WIND FIELDS

MURILO AUGUSTO PINHEIRO, MSc

The University of Texas at Arlington, 2019

Supervising Professor: Dr. Yan Wan

This work focuses on the roles of on-board sensing and off-board sensing through wireless communication for UAV missions. Employing UAV path planning under spatiotemporal wind effect as a case study, this work implements a modeling framework composed by the vehicle dynamics, environmental effect and communication model that transmits wind field data. Based on the analysis of the minimum-time optimal UAV path planning solution under communication constraints and spatiotemporal wind impact, this work obtains quantitative insights into the effect of communication quality and information update configuration on the performance of path planning. This study finds that on-board sensing and off-board sensing can both enhance the planning performance, however the performance of off-board sensing deteriorates as the communication conditions progressively get worse. Moreover, the path planning performance can be optimized if the information update parameters are correctly chosen subject to the channel capacity constraints. Ultimately, this work designs and validates an UAV navigation system which is an initial and essential step for a

practical implementation of the path planning developed in this document. Partial results of this thesis were included in Paper [1].

TABLE OF CONTENTS

LIST OF ILLUSTRATIONS

LIST OF TABLES

# CHAPTER 1

# INTRODUCTION

## 1.1 Introduction

Unmanned aerial vehicles (UAV) were initially developed for military applications and to execute missions that are dangerous or dirty. With the recent technological advances and consequently cost reduction of its components, the usage of UAV has been rapidly extended to a wide range of scientific, commercial and civilian applications.

As a part of a moving aerial platform, UAVs carry communication, sensing, computing and control components [2]. However, these platforms are often constrained on the availability of power resources on-board as well as how much weight and size of equipment it can carry. Thus, performing all computing and sensing functionalities on-board becomes impractical for these aerial vehicles [3]. Alternatively, communication of useful information to on-board UAV systems through wireless communication from off-board sensing and computing devices at ground stations or even at other UAVs becomes a possible solution. However, this alternative raises several questions that are yet to be answered on the roles of on-board and off-board sensing and computation. Some of these questions are related to the benefit of off-board information for specific UAV missions, the impacts of communication imperfection and the optimal configuration of the communication services to optimize the overall mission performance. The answers for these questions can lead to guidelines for UAV traffic management (UTM) to define the levels of responsibilities, the overall management architectures, and the missions of UAV information service providers. The goal of

this work is to investigate the roles of on-board sensing and off-board sensing through wireless communication for UAV missions using a quantitative analysis. Such analysis is motivated by achieving a better understanding on the benefits of communication as well as the effects of imperfect communication on UAV missions. To do that, an UAV mission composed by a path planning under wind conditions task is employed as a test bed for this study. Currently, most UAV path planning solutions do not consider the knowledge of weather conditions [4], which if exploited, can potentially improve the effectiveness of path planning solutions [5]. Such weather conditions can be obtained using on-board wind sensors [6] or provided by UAV information service providers such as UAV weather stations [7]. Per the best of the current knowledge, there are no prior studies that focus on understanding the effects of on-board/off-board sensing and communication performance on UAV path planning. In the next paragraph, there is a review about the works in the literature that are related to three aspects of this study, including path planning, wind impact, and UAV wireless communication.

On the aspect of path planning, many studies have been conducted on designing path planning algorithms in different environments [8, 9, 10, 11]. Here in this work, a minimum-time trajectory planning in a spatiotemporal wind field is considered. Related to this direction, Paper [8] considers a tour planning for an unmanned aerial vehicle that operates in a spatiotemporal wind environment. The author iteratively calculates the minimum-time trajectory based on the Dubins theorem, by computing a new heading angle that counteracts the wind effect on the aerial vehicle. Papers [9] and [10] based their work on the well-known Zermelo's navigation problem. In paper [9], the Zermelo's problem is not only implemented to find the minimum-time trajectory of a vehicle moving under wind influence between two locations but also to avoid the vehicle to enter restricted areas, while in [10], the Zermelo's problem

solution is combined to a travelling salesman problem to plan the shortest trajectories for an UAV to execute structure inspections in windy environments. In addition, studies such as [12] and [13] developed optimal path planning in windy environments using different optimization strategies and objective functions. The author of Paper [12], implements a wind-optimal path planning based on Ordered Upwind Method that incorporates obstacle avoidance, while Paper [13] implements an algorithm to minimize the energy consumption of an electric aerial vehicle using markov decision processes.

Wind impact can be modeled as stochastic spatiotemporal spread processes [14, 15]. Wind information can be measured on-board using an anemometer or locally estimated using a conventional UAV on-board sensor suite [16, 17, 18]. However, these approaches are limited in terms of sensing range and accuracy. Alternatively, weather service providers can potentially provide wind forecasts that cover larger areas through wireless communication [5]. In the latter case, the range, update, and fidelity of wind information are dependent on communication channel characteristics.

Communication is essential to allow weather stations and base stations to be employed as off-board sensors as well as to provide UAVs with higher performance computing units. The performance of the communication system is directly related to the spectrum being allocated and differently from ground communication, the Air-to-Ground (A2G) channel characteristics are influenced by the altitude, type of UAV, elevation angle and propagation environment conditions [19, 20]. Given the high flexibility and mobility of UAVs, its employment in wireless network applications has recently drawn significant attention from the community. The applications in study include the enhancement of communication coverage and capacity, flying UAVs for emergency communication, UAV-to-UAV communication, among others [3, 19, 21, 22, 23, 24, 25]. For these applications, recent advances include wire-

less channel modelling and performance analysis, resource management and energy-efficiency, trajectory optimization to enhance communication, and among others (see e.g., [21, 26]).

The contributions of this work are summarized as follows. First, a complete modeling framework that includes the communication channel, vehicle dynamics, and environmental impact, is constructed to understand the roles of on-board/off-board computing through wireless communication. Second, a minimum-time optimal UAV path planning solution under communication constraints and spatiotemporal wind impact is developed. Third, this optimal path planning is used as a case study to understand the trade-off between wind information availability, i.e. range and update rate, and communication quality in terms of bit error rate (BER), packet error rate (PER) and capacity. Ultimately, to complement the theoretical study developed in this thesis, a navigation system for UAV is designed and validated. A navigation system is vital for measuring and estimating UAV states and thus a control system can be designed in order to allow stable flights, autonomous navigation and, in special, the implementation of the path planning considered in this work.

The paper is organized as follows. Chapter 2 includes the modeling framework for the communication system, which consists of the Air-to-Ground channel model and physical layer of the IEEE802.16 protocol. Chapter 3 details the aerial vehicle dynamics, the wind dynamics, two approaches for preparing the received wind data and finally describes the path planning algorithm implemented to be used as the test bed. Chapter 4 includes the analytical results. Chapter 5 describes the navigation system design, implementation and validation. Finally, Chapter 6 concludes this document, summarizing and discussing the outcomes of this work along with a brief description of future work.

# CHAPTER 2

# WIRELESS AIR-TO-GROUND COMMUNICATION MODEL

This chapter describes the wireless UAV-to-Ground communication model. It firstly presents a description of the Air-to-Ground channel model used to calculate the channel performance. Next, it defines the channel performance by measuring the signal-to-noise ratio (SNR) and the channel capacity. Then, the UAV-to-Ground communication is described using the IEEE802.16 communication protocol.

## 2.1 Air-to-Ground Channel Model

The Air-to-Ground (A2G) channel model describes the path attenuation along the communication channel from a UAV to the ground station.

### 2.1.1 Propagation Modes

The channel model is based on the Line-of-Sight (LOS) or Non-Line-of-Sight (NLOS) propagation modes. As presented in the literature [19, 22, 27, 28, 29, 30], the model is described by a path attenuation, which is represented by a probabilistic combination between each propagation mode. Each mode is composed by a free-space path loss and a shadowing term that is dependent on the environment. Each mode has a probability of occurrence decided by the UAV's elevation angle and environment parameters such as the buildings' density and height. Figure 2.1 illustrates the two propagation modes.

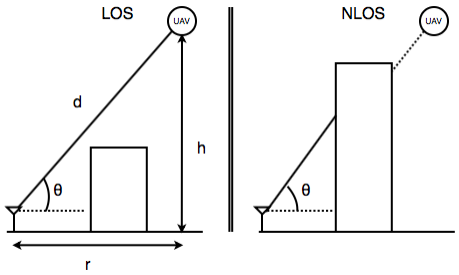


Figure 2.1: Air-to-Ground channel propagation modes

Denote the occurrence probability of the LOS and NLOS propagation mode as $P_L$ and $P_N$ respectively, we have

$$P_L + P_N = 1. \tag{2.1}$$

When compared to terrestrial channels, air-to-ground channels are more likely to have a LOS component. Thus, models such as Rician, large scale Rayleigh, and free-space path loss are commonly utilized in the air-to-ground channel literature. A downside of these models is that they are not capable of addressing environmental impacts on the line-of-sight event [27]. Later, one of the most complete model on the effects of building blockage on electromagnetic wave attenuation was proposed in [31] and the authors of [19] incorporated it into a probabilistic Line-of-Sight air-to-ground channel model in urban environments.

In an urban environment where the effects of buildings are non-negligible, $P_L$ is modeled as [19]

$$P_L(\theta) = \frac{1}{1 + Ae^{(-B(\theta - A))}}, \tag{2.2}$$

where $\theta$ is the elevation angle, $A$ and $B$ are environment-dependent coefficients dependent on the ratio between constructed land area and the total area, the average number of building per unit of area, and a scaling parameter that describes the distri-

bution of the buildings' heights according to a Rayleigh probability density function. The elevation angle is decided by the horizontal distance $r$ between UAV and ground station and by the UAV's height $h$ as [19],

$$\theta = \tan^{-1}(\frac{h}{r}). \tag{2.3}$$

The probability of NLOS mode is then be derived according to Equation (2.1) as

$$P_N(\theta) = 1 - P_L(\theta) \tag{2.4}$$

### 2.1.2 Path Loss Models

The electromagnetic wave propagation attenuation, or path loss, is defined in dB, as the difference between the transmitted and received signal power. The representation of the path loss is captured in the equation 2.5 [32]:

$$L = 10\log_{10}(\frac{P_t}{P_r}). \tag{2.5}$$

Generally, the path loss is a positive number which means that the power of the receiving signal is always lower than the power of the transmitted signal since the channel does not contain active elements. Path loss attenuation is composed by two elements: the free-space path loss $L_f$ and the shadowing effects $L_s$ [33],

$$L = L_f + L_s. \tag{2.6}$$

The free-space path loss captures the energy attenuation when the electromagnetic waves travels in the free space and it accounts exclusively for the LOS propagation mode [32]. The free-space path loss is modeled as [33]

$$L_f(d) = 20\log_{10}(d) + 20\log_{10}(\frac{4\pi}{c}) + 20\log_{10}(f_c + f_D). \tag{2.7}$$

where $d$ is the propagation distance in meters, $c$ is the speed of light in m/s, and $f_c$ is the electromagnetic wave's frequency in hertz, $f_D$ is the frequency shift caused by the Doppler spread effect. Note that for a mobile source, the electromagnetic wave's frequency is affected by the Doppler effect. Different from applications which the UAV is capable of being stationary such as [29], [30], [34], mobile applications are sensitive to the relative velocity between transmitter and receiver. Thus, the air-to-ground channel model used in this document should account for this effect. The maximum frequency shift caused by the UAV relative movement is modeled as

$$f_D = v\frac{f_c}{\lambda}, \tag{2.8}$$

where $v$ is the UAV's velocity, and $\lambda$ is the wavelength of the electromagnetic wave.

The path loss caused by shadowing effects, $L_s$, captures the energy attenuation of the electromagnetic wave considering the random signal blockage and changes in scattering obstacles and reflecting surfaces, and is modeled as

$$L_s = P_L L_{s_L} + P_N L_{s_N}, \tag{2.9}$$

where $L_{s_L}$ and $L_{s_N}$ are the path losses caused by shadowing effects in the LOS and NLOS propagation modes respectively. In the LOS propagation model, the path loss caused by shadowing effects, $L_{s_L}$, is empirically modeled as [33]

$$L_{s_L} = \mathcal{N}(0,\, 4). \tag{2.10}$$

where $\mathcal{N}(\mu_L, \sigma_L^2)$ is the normal distribution with mean $\mu_L$ and variance $\sigma_L^2$.

On the other hand, for the NLOS propagation model, the path loss caused by shadowing effects is modeled as [33]

$$L_{s_N} = \mathcal{N}(0,\, 10) + \mathcal{N}(\frac{-94.2 + \theta}{-3.44 + 0.0318\theta},\, \frac{-89.55 + \theta}{-8.87 + 0.0927\theta}). \tag{2.11}$$

Although shadowing is often modeled as a random variable with Gaussian distribution, the work presented in this document is mainly concerned with its expected value instead of its random characteristic.

### 2.1.3 Channel Performance Model

The wireless channel performance can be characterized in terms of the signal-to-noise ratio (SNR). The SNR in $dB$ is defined as the difference between the received power and noise power [35],

$$S = P_r - P_n = P_t + G_t + G_r - (L + N_p), \tag{2.12}$$

where $P_t$ is the transmitting power, $G_t$ and $G_r$ are the gains of the transmitting and receiving antenna respectively. For a conservative calculation, both antenna gains are assumed to be 0 $dBi$. $N_p$ is the noise power at the receiver, which it is a function of the Boltzmann constant $(K)$, temperature $(T)$, bandwidth, $(BW)$, and noise figure $(N)$,

$$N_p = 10 \log_{10}(KTB_W) + N \tag{2.13}$$

Another widely-used channel performance indicator is the channel capacity $(C)$, which is defined as the maximum data rate that can be transmitted through the communication system [20, 35]. The capacity is modeled from the well-known Shannon-Hartley theorem as [35]

$$C = B_W \log_2(1 + S), \tag{2.14}$$

where $C$ is the capacity in bits per second, $B_W$ is the bandwidth in $Hz$ and $S$ is the dimensionless SNR.

### 2.1.4 Channel effect on the transmitted signal

In the air-to-ground channel modeled, the transmitted signal may be corrupted by the wireless channel. The received signal is given by $r(t) = s(t)+n(t)$, where $s(t)$ is the transmitted signal and $n(t)$ is a white Gaussian noise with zero mean and standard deviation $\sigma$. The noise standard deviation, $\sigma$, is a function of the signal-to-noise ratio and one can calculate it using the following expression:

$$\sigma = \sqrt{\frac{\frac{1}{T}\int_0^T s^2(t)dt}{S}} \tag{2.15}$$

## 2.2 Communication model

The communication model employed in this work is inspired by the IEEE802.16 standard, selected by NASA as a promising technology for UAS Control and Non-Payload Communications (CNPC) link [36]. The standard [37] defines both physical and medium control access (MAC) layers. For simplicity, the work described in this document only implements the IEEE802.16 physical layer. The proposed system is composed by two communicating nodes, and thus the upper layers in the communication stack can be summarized to a protocol that creates packets of bits and that implements some sort of error detection.

To begin with the communication system model overview, the input data, in this case the wind map, is converted to a bit stream to allow the information to be transmitted. The wind map is represented by two matrices that capture the wind speed in the longitudinal and latitudinal directions and their length varies according to the range and resolution of the available wind information. Each matrix is transformed into a vector by concatenating its rows together and then each value to be transmitted is converted to binary number using $m$ bits for quantization plus

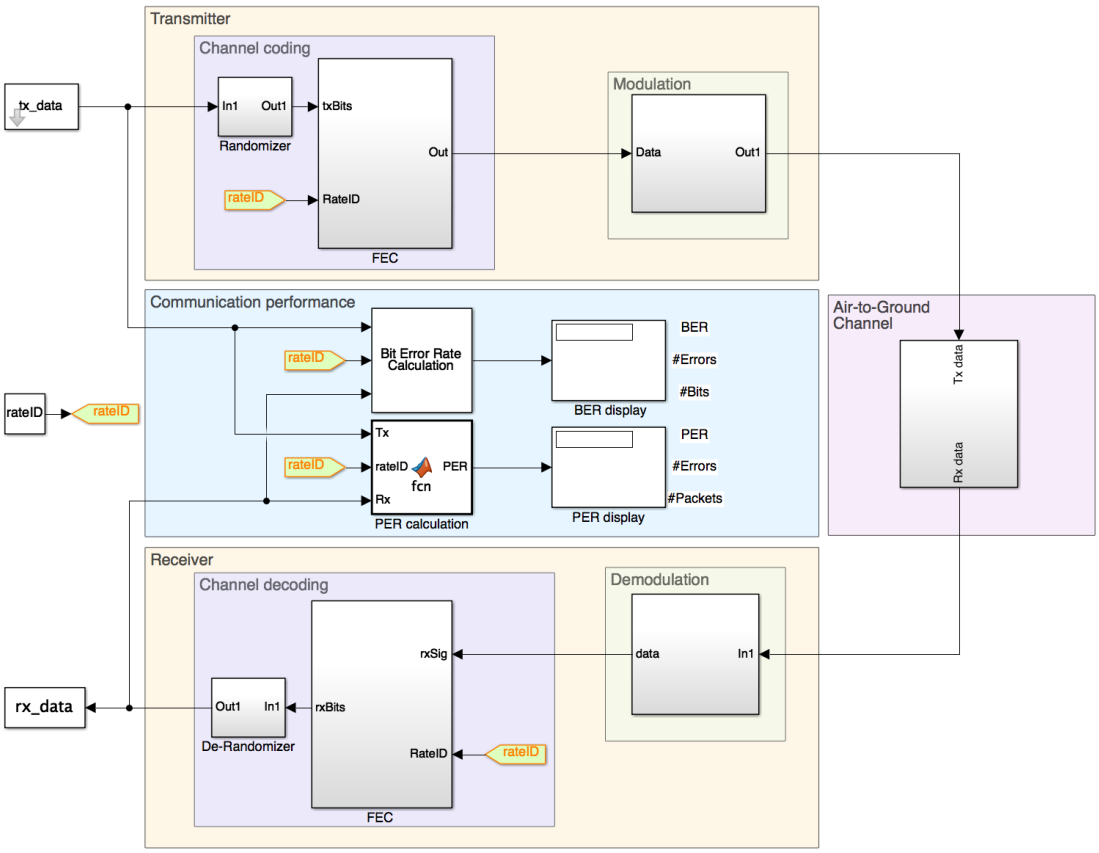


Figure 2.2: Block diagram representing the physical layer of the communication system model

1 bit for representing the sign, making a total of $m + 1$ bits per value. The bit sequence generated is then grouped into packets of size $L$ and a cyclic redundancy check (CRC) is added to the packet to allow the receiver to detect whether the information is correctly received or not.

The overall purpose of the communication system is to transmit information, in this case, the wind field data, from the weather station to the UAV. The block diagram of the communication system, presented in Figure 2.2, is composed of four main blocks: transmitter, air-to-ground channel, receiver and communication performance, which their functions are described in details below.

The transmitter block receives the data to be transmitted in a data stream format (expressed as $tx\_data$ in the diagram), and its functionality is to convert the incoming message into a modulated signal to be transmitted. The process is composed of 2 sub-blocks, channel coding and modulation. Channel coding is composed of a randomizer, which scrambles the data stream to avoid long runs of zeros or ones and hence facilitates the synchronization procedure between the transmitter and receiver. The other sub-block is the FEC which stands for Forward Error Correction. The FEC is responsible for improving the communication performance and robustness against channel impairments by allowing the communication system to detect and correct random errors as well as burst errors. In particular, such improvement is due to the fact that FEC generates $N$ redundant bits for every sequence of $K$ bits. Thus, it allows an effective code rate of $K/(N + K)$. In addition, FEC guarantees that adjacent subcarriers are mapped with nonadjacent coded bits wand neighbor bits are alternately mapped into less or more significant of the constellation, thus avoid long sequences of unreliable bits. Next, the modulation block modulates the information to be transmitted in the carrier frequencies. The modulation is performed using any of the following modulation techniques: BPSK, QPSK, 16-QAM and 64-QAM. The IEEE 802.16 standard supports an adaptive modulation/coding mechanism to allow the transmission rate to vary according to the channel conditions, however, for consistency of results, the model employed in this work does not allow adaptive modulation/coding. Instead, it allows the user to select its desired modulation in. In this work, BPSK modulation with a coding scheme with rate 1/2 is selected in the rateID block. After the information is modulated, the data symbols are mapped onto 256 sub-carriers using an inverse fast fourrier transform and a cyclic prefix is inserted to result in the OFDM symbols to be transmitted over the wireless channel.

The air-to-ground block implements the probabilistic air-to-ground channel describe in Section 2.1, which takes as an input the modulated sub-carriers from the transmitter block and output the data corrupted with noise.

The receiver block receives the noisy subcarriers from the channel and processes it to retrieve the transmitted information. It is composed of two sub-blocks: demodulation and channel decoding. Demodulation sub-block removes the cyclic prefix and applys the fast Fourier transform to map the OFDM symbols back to the modulated data symbols. The channel decoding sub-block, composed of the FEC and de-randomizer, decodes the information and de-scrambles channel decoding input into the messages received by the UAV.

The communication performance block evaluates the performance of the communication system (i.e., bit error rate (BER) and packet error rate (PER)) by comparing the transmitted and received data streams. BER is calculated by dividing the number of bits received in error by the total number of bits transmitted, while PER is analogically obtained using the number of packets instead of the number of bits. In this work, each packet includes 88 bits (80 data bits and 8 redundant bits), the maximum number of bits that can be transmitted each time. Figure 2.3 shows the performance of the communication system in terms of the channel SNR. It can be seen from the figure that 1) both BER and PER decrease with the increase of SNR; 2) with the same SNR value, the BER is always smaller than PER. Once the information is received, each packet is checked and discarded if an error is detected, and finally, the received data is converted to decimal representation, and reorganized back as the original matrices.

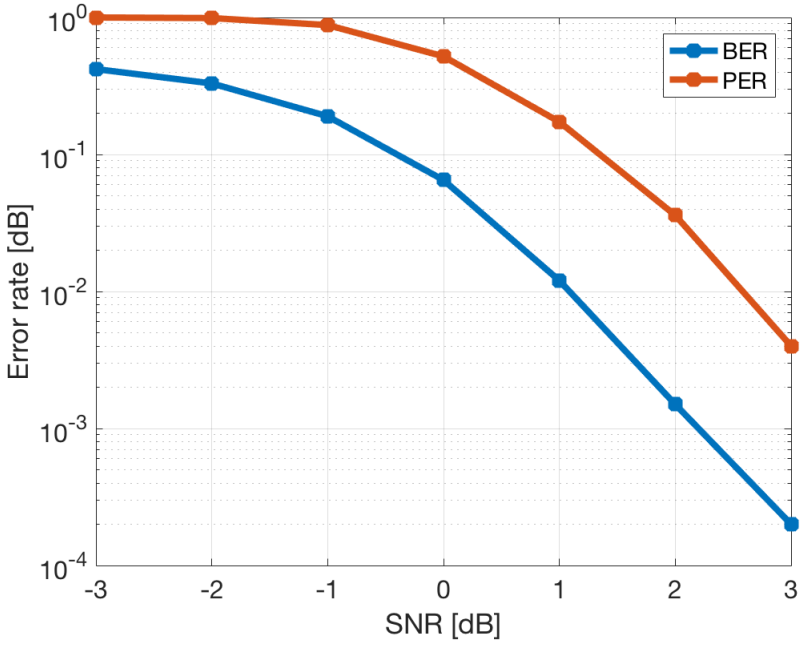


Figure 2.3: Communication performance vs channel performance

# CHAPTER 3

# PATH PLANNING IN A WIND FIELD

The minimum-time path planning algorithm designed in this document is based on the Zermelo's navigation problem. This problem is named after a German mathematician called Ernst Zermelo. In 1931, he proposed the problem of a ship moving with constant speed relative to the water while considering the its current with the goal to navigate from point A to point B in minimum-time by utilizing the currents in its favor [38]. Despite of the original formulation, this problem is widely known in its aircraft version which the water currents are replaced by the wind fields. Thus, the Zermelo's problem represents a milestone for aerospace and aviation engineers to study guidance and control problems [9]. Next, the UAV and wind models are introduced along with the path planning algorithm description.

## 3.1 UAV dynamics

Consider a UAV flying from point A to point B in a two dimensional airspace. The UAV dynamics can be modeled as:

$$\begin{cases} \dot{x}(t) = v(t)\cos\phi(t) + W_x(x,y,t) \\ \dot{y}(t) = v(t)\sin\phi(t) + W_y(x,y,t) \end{cases}, \tag{3.1}$$

where $x(t)$ and $y(t)$ is the position of UAV in $x$ and $y$ axis respectively. $v(t)$ is the UAV's speed, and is assumed to be constant $v(t) = V$. $\phi(t)$ is the UAV's heading angle. $W_x$ and $W_y$ are wind speed in $x$ and $y$ axis respectively.

For this particular study, a spatiotemporal wind dynamics that captures twisted wind spread in all directions is used with the purpose of studying spatiotemporal wind impact to the performance of path planning.

$$\begin{cases} W_x(x,y,t) = |W| y \cos(\omega t + \psi_0) \\ W_y(x,y,t) = |W| x \sin(\omega t + \psi_0) \end{cases}, \tag{3.2}$$

where $|W|$ is the amplitude of wind speed at location $(1,1)$. To make sure that the UAV's speed is greater than the wind's speed, we have $|W|y < V$ and $|W|x < V$. $\omega$ is the change rate of the wind direction, and $\psi_0$ is the wind's initial direction at $t = 0$. Figure 3.1 illustrates examples of the spatiotemporal wind field modeled when $|W| = 0.01$. Different wind field behaviors can be generated as $\omega$ and $\psi_0$ vary.

## 3.2 Received wind data preparation

Two approaches are considered to process the received wind field data subject to errors caused by the communication process. In approach 1, the received data is directly used. In approach 2, the error information (i.e., the received packet) is discarded. The two approaches correspond to the two performance indicators that measure the error information: BER and PER respectively. For each of these two approaches, a simple filtering procedure is used to process the received wind field data to prepare for path planning. To describe it, the wind map should be defined as a grid, in which each grid contains the wind speed for a location in the map. Thus, an averaging filter with size $m$ takes the average of the closest $(2m+1)^2$ grids around each grid in the map to account for the errors and loss of data. The wind speed values near the edges of the map, in which do not have $(2m+1)^2$ neighbors, are discarded. Figure 3.2 exemplifies this data preparation procedure.

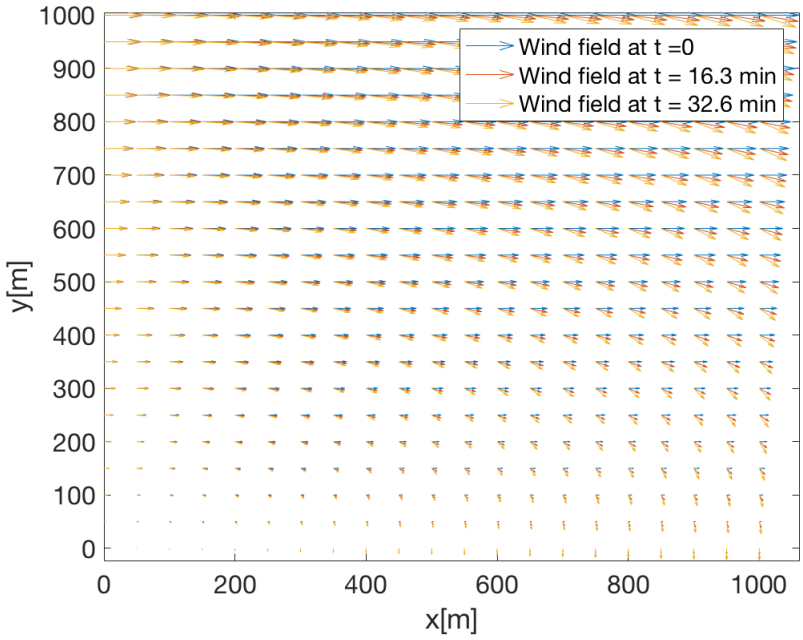


(a) $\omega = -0.01$ rad/s and $\psi_0 = 0$ rad

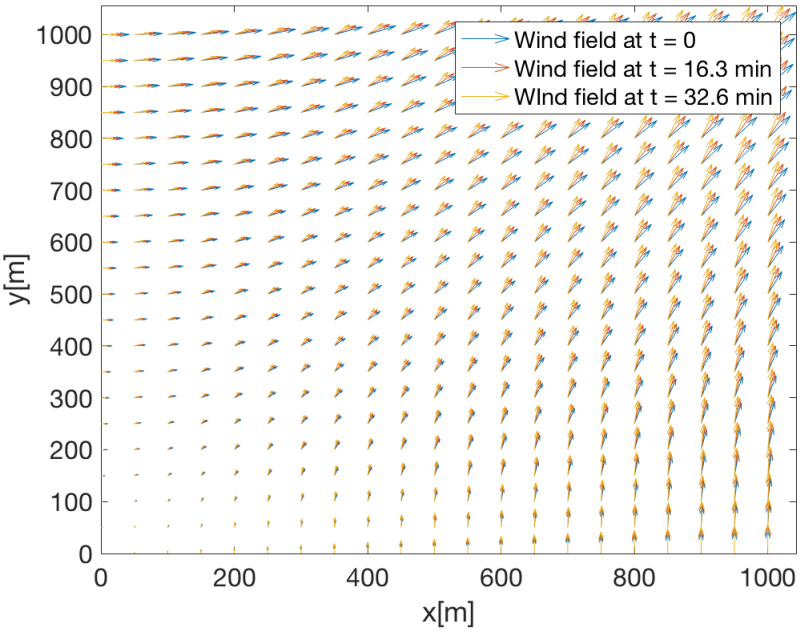


(b) $\omega = 0.01$ rad/s and $\psi_0 = \frac{\pi}{2}$ rad

Figure 3.1: Examples of the spatiotemporal wind field

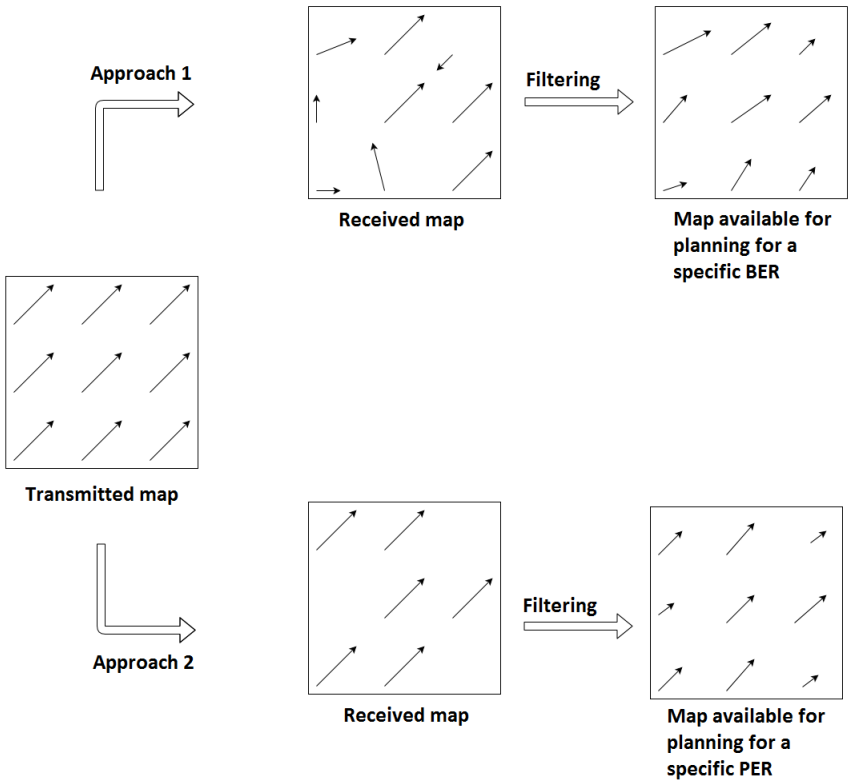


Figure 3.2: Differences between BER and PER approaches on the wind field data preparation

At this point there is a need to differentiate the real wind information from the wind information available to be used during path planning. Thus, the physical wind data is referred to as wind field data, while the later as wind map data. As the wind field is unlimited in terms of space, a parameter called range is defined. This parameter delimits the amount of information that the wind map contains. Moreover, due to the time-varying behavior of the wind field, there is a need to also define a parameter called update, in which it captures the wind field at a given time instant. Thus, the wind field data can be converted into the wind map to be used during the UAV path planning. Since the range of the transmitted wind field information may not cover the entire airspace or the wind map resolution is limited,

an extrapolation/interpolation method should be used to estimate the missing wind information. In particular, the unknown wind information is obtained by using the nearest-neighbor method. For such method, the wind speed at a particular location that is not defined by the grid will be equal to the wind speed value such that the distance between this location and its adjacent grid locations is minimum.

## 3.3 Path planning

Consider the dynamics described in Equation (3.1). The goal is to find the optimal $\phi(t)$ to minimize the cost time for a UAV traveling from the initial position to the destination (see Figure 3.3). The wind information is provided through the Air-to-Ground communication.

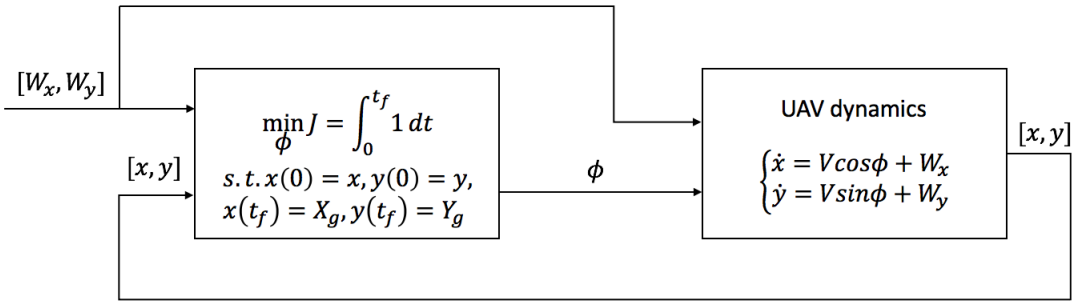


Figure 3.3: The block diagram of the UAV control system.

Mathematically, the problem is formulated as [9]:

$$\min_{\phi} J = \int_0^{t_f} 1dt \tag{3.3}$$

$$s.t. \quad x(0) = X_0, \quad y(0) = Y_0,$$
$$x(t_f) = X_g, \quad y(t_f) = Y_g \ , \tag{3.4}$$

where $(X_0, Y_0)$ and $(X_g, Y_g)$ are the UAV initial position and the destination position respectively.

Given the cost function $J$ and the UAV dynamics shown in Equation (3.1), the Hamiltonian of the system is [9]:

$$H = \lambda_x(Vcos\phi + W_x) + \lambda_y(Vsin\phi + W_y) + 1 \tag{3.5}$$

where, $\lambda_{|.|}$ is the Lagrange multiplier. Thus, the costate equations are [9]:

$$-\dot{\lambda_x} = \frac{\partial H}{\partial x} = -\lambda_x \frac{\partial W_x}{\partial x} - \lambda_x \frac{\partial W_y}{\partial x} \tag{3.6}$$

$$-\dot{\lambda_y} = \frac{\partial H}{\partial y} = -\lambda_x \frac{\partial W_x}{\partial y} - \lambda_x \frac{\partial W_y}{\partial y} \tag{3.7}$$

$$\frac{\partial H}{\partial \phi} = V(-\lambda_x sin\phi + \lambda_y cos\phi) = 0 \tag{3.8}$$

Therefore, the Lagrange multiplier can be obtained from Equations (3.5) and (3.8) as [9]:

$$\lambda_x = -\frac{-cos\theta}{V + W_x cos\phi + W_y sin\phi} \tag{3.9}$$

$$\lambda_y = -\frac{-sin\theta}{V + W_x cos\phi + W_y sin\phi} \tag{3.10}$$

Equations (3.9) and (3.10) can be combined either to (3.6) or (3.7) to obtain:

$$\dot{\phi} = sin(\theta^2)\frac{\partial W_y}{\partial x} + sin\phi \cos\phi(\frac{\partial W_x}{\partial x} - \frac{\partial W_y}{\partial y}) - cos(\phi^2)\frac{\partial W_x}{\partial y} \tag{3.11}$$

The solution of (3.11) (denoted as $\phi^*$), is the optimal control sequence which allows the UAV to traverse from its initial location to the target location in minimal time.

Denote the length of the optimal control sequence as $K$, then the samples in the sequence are spaced by $t_f/K$ seconds.

Different approaches have been developed to minimize a cost function with fixed initial and final time. However, the cost function described in Equation (3.4) is a free-final time problem. The common method to solve such problem is to transform the free-final time optimal control problem to a fixed-final time problem by re-scaling the time variable $t$, into the re-scaled time variable $\tau$, where $\tau = t/t_f$. With this re-scaling, $\frac{d}{dt}$ should be substituted by $\frac{1}{t_f}\frac{d}{d\tau}$ [38].

Once the optimal control input sequence $\phi^*$ is found, it is inputted into the vehicle dynamics to obtain the vehicle trajectory. After each control input sample is inputted, the algorithm checks if there is an update in the wind map information. If a new map is available, then a new control sequence is recomputed and applied into the vehicle. Note that the control input is calculated based on the wind information provided by the communication system, which may lead to inaccurate information considering the sensor range, quantization error and imperfect communication. If the vehicle does not reach the goal within certain accuracy, the control is then implemented again based on the current vehicle position and wind map, until it reaches the goal or there is a new wind map update (see Algorithm 1). Figure 3.4 shows two examples of the planned path using the proposed algorithm, in which the circles represents the wind information range and the number of circles represents how many wind map updates were present during the planning.

**Algorithm 1** Path planning algorithm

1: Set trajectory parameters (i.e.,UAV's initial position, goal, and speed, and sample number $K$), wind map parameters (map range and update rate).

2: Get vehicle current location and set j=1

3: Transmit wind map through A2G channel.

4: Find $\phi^*$ and $t_f$ based on the rceived wind map by solving Equation 3.11.

5: For each $j \leq K$,

if there is a new map update

do step $2-4$

if there is no map update

input the $j$-th sample control policy to the vehicle model.

6: Repeat step $2-5$ until the goal is reached.

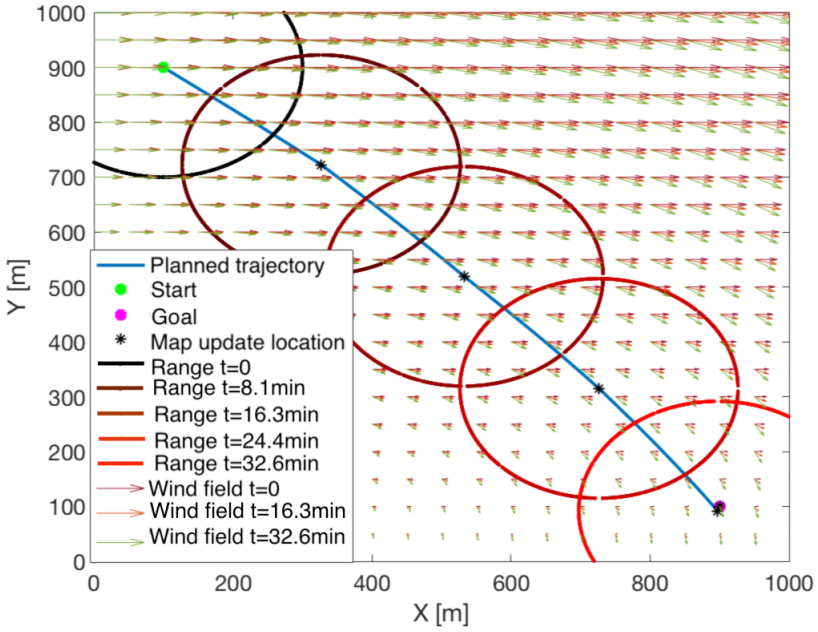


(a) range = 200m and update rate = 0.1225 updates/min

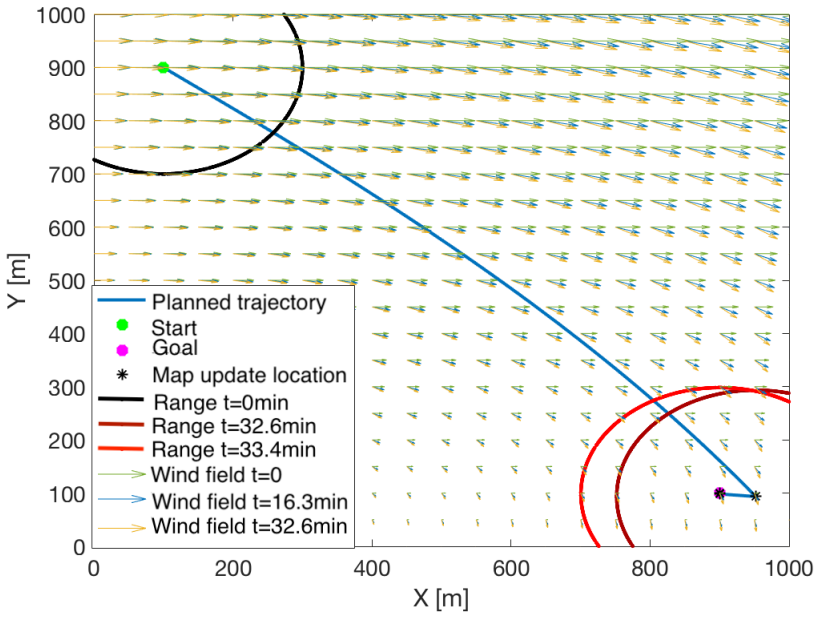


(b) range = 200m and update rate = 0.0306 updates/min

Figure 3.4: Planned trajectory duration for spatiotemporal wind

# CHAPTER 4

# ANALYSIS ON ON-BOARD AND OFF-BOARD SENSING FOR UAV PATH PLANNING

Initially, the path planning performance in a perfect communication environment is studied. In this context, perfect communication is assumed in the sense that that the wind field data is not corrupted with noise originated by the wireless channel. When the sensing range is small and update rate is high, this perfect communication case corresponds to on-board sensing as no communication issue exists. The relation between the path planning performance and wind information update parameters (including update rate and range) are studied. Then, the imperfect communication and off-board sensing is considered, and the path planning performances are further studied with different communication environment set-ups (e.g., different SNRs).

## 4.1 On-board sensing and perfect communication

In the case of perfect communication environment or onboard sensing, two wind scenarios are studied, the time-invariant spatial wind and the spatiotemporal wind. For these two scenarios, the relation between the path planning performance and the information update parameters (i.e. update rate ($r_u$) and map range ($l_m$)) are studied respectively. The simulation settings in both scenarios are summarized as follows. The initial location of the UAV is set as $(X_0, Y_0) = (100, 900)$, and the destination is $(X_g, Y_g) = (900, 100)$. The UAV's velocity is set as $v = 0.5m/s$. The wind magnitude is $|W| = 0.01$, and the wind direction change rate is $\omega = 0$ in the

Table 4.1: Comparison of the path planning performances

| **Scenario settings** | **cost time with wind information** | **cost time without wind information** | **difference** |
|---|---|---|---|
| $\omega = -0.01$ and $\psi_0 = 0°$ | 31.57 $(min)$ | 46.12 $(min)$ | 14.55 $(min)$ |
| $\omega = -0.01$ and $\psi_0 = 90°$ | 41.87 $(min)$ | 47.97 $(min)$ | 6.10 $(min)$ |
| $\omega = -0.01$ and $\psi_0 = 180°$ | 44.81 $(min)$ | 45.96 $(min)$ | 1.15 $(min)$ |
| $\omega = -0.01$ and $\psi_0 = 270°$ | 33.52 $(min)$ | 46.91 $(min)$ | 13.39 $(min)$ |
| $\omega = 0.01$ and $\psi_0 = 0°$ | 34.16 $(min)$ | 46.97 $(min)$ | 12.81 $(min)$ |
| $\omega = 0.01$ and $\psi_0 = 90°$ | 43.90 $(min)$ | 46.97 $(min)$ | 3.07 $(min)$ |
| $\omega = 0.01$ and $\psi_0 = 180°$ | 41.74 $(min)$ | 45.52 $(min)$ | 3.78 $(min)$ |
| $\omega = 0.01$ and $\psi_0 = 270°$ | 32.08 $(min)$ | 47.56 $(min)$ | 15.48 $(min)$ |
| average | 37.96 $(min)$ | 46.75 $(min)$ | 8.79 $(min)$ |

spatial wind scenario, and $\omega = 0.01$ or $-0.01$ in the spatiotemporal wind scenario. The initial wind direction is set as $\psi_0 = 0°$, $90°$, $180°$ and $270°$ respectively.

Figures 4.1a and 4.2b show the relation between the path planning performance and the update parameters in average spatial wind scenarios (i.e., the average of scenarios with different $\psi_0$) and average spatiotemporal wind scenarios (i.e., the average of scenarios with different $\psi_0$ and $\omega$), respectively. It can be seen from the figures that: 1) in both scenarios, the cost time decreases with the increase of the update rate and the map range; 2) compared to the spatiotemporal wind scenario, the spatial wind scenario leads to less cost time, indicating better path planning performance.

Moreover, the improvement of path planning performance with the sensed (or transmitted) spatiotemporal wind information is further studied. To do that, we compare the cost time for the UAV traveling from the initial position to the destination when 1) the wind information is available, and then 2) the wind information is not available. When the wind information is available, the information update rate is set as $r_u = 0.1225$ per minute, with the map range $l_m = 1000m$. The results are shown in Table 4.1.

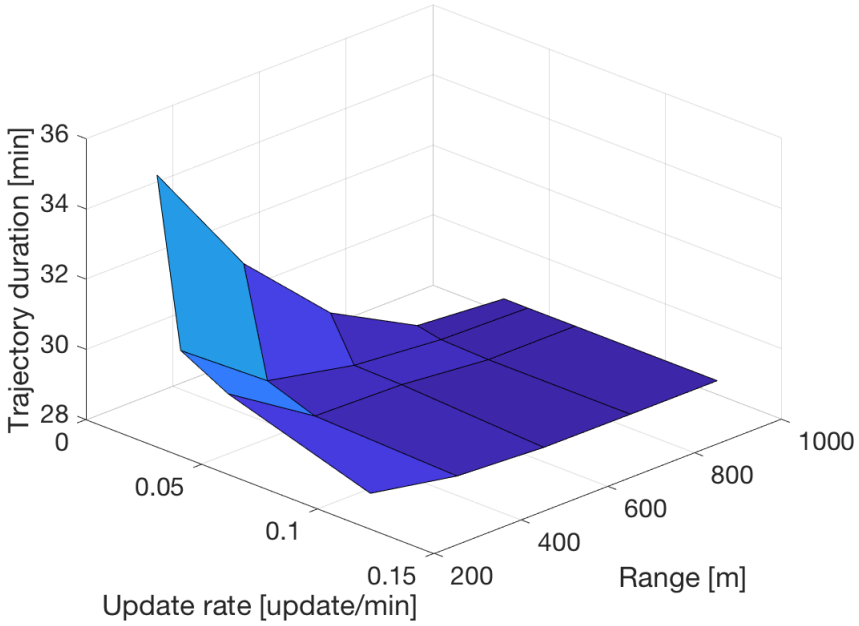


(a) Spatial wind scenario

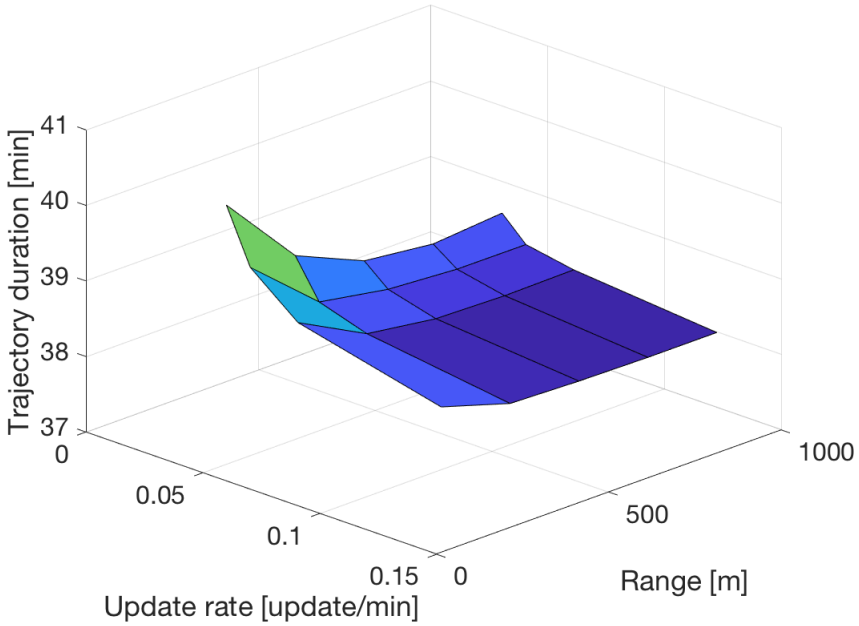


(b) Spatiotemporal wind scenario

Figure 4.1: Effect of wind information availability on the planned trajectory duration for perfect communication scenarios

It can be seen from Table 4.1 that 1) in all scenarios, the cost time is reduced when the wind information is provided; 2) the performance is improved more (larger difference) when the wind direction is consistent with desired UAV heading direction (i.e., when $\psi_0 = 0°$ and $\psi_0 = 270°$).

## 4.2 Off-board sensing and imperfect communication

In this section, the path planning performance with imperfect communication is studied. The UAV trajectory parameters and the wind scenarios are the same with the settings in Section 4.1. Note that all figures are derived from the average of all wind scenarios with different $\psi_0$ and $\omega$.

Figures 4.2a and 4.2b show the path planning performance with different communication performance (i.e., different SNR) when the wind update parameters are set as $r_u = 0.1225$ per minute, and $l_m = 1000m$. Figure 4.2a is derived by processing the received data from approach 1, which is described in Section 3.2 (corresponding to BER), and Figure 4.2b is derived from approach 2 (corresponding to PER). When the SNR is greater than 3dB, the BER and PER are equal to zero, and therefore the communication can be considered perfect. It can be seen from the figure that: 1) the cost time decreases with the increase of the SNR in both cases; 2) the path planning performance is improved (i.e., less cos time) in all SNR cases, compared to the non-available wind information case listed in the third column in Table 4.1.

Next, the relation between the path planning performance and the wind update parameters in different SNR cases is evaluated. Figure 4.3 shows the path planning performance with different map update rates and map ranges, in different PER cases. It can be seen that 1) in all PER cases, the cost time decreases with the increase of the update rate and wind map range; 2) with the same update rate and wind map range, the cost time increases with the increase of PER. Figure 4.4 shows the path

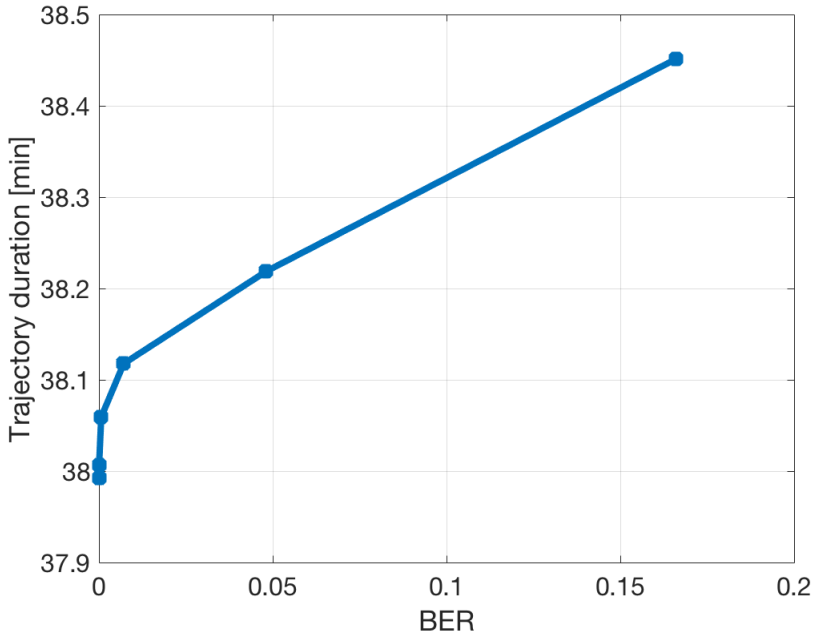


(a) Using approach 1: BER

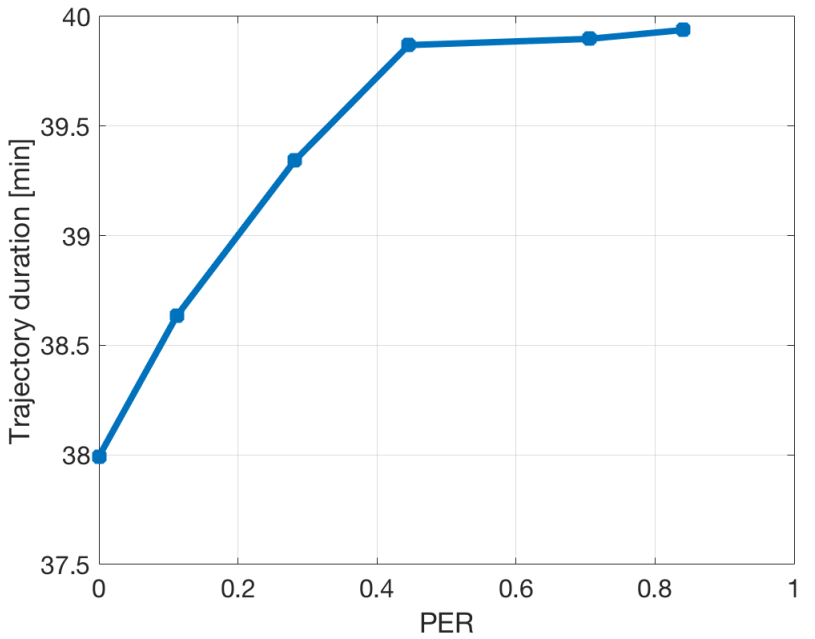


(b) Using approach 2: PER

Figure 4.2: Trajectory duration with different communication performance

planning performance with different map update rates and map ranges, in different BER cases. Similarly, in all BER cases, the following observations can be made: 1) the cost time decreases with the increase of the update rate and wind map range; 2) with the same update rate and wind map range, the cost time increases with the increase of BER.

The wind map range and update rate (interpreted as configuration of the weather service provision) can also be optimized when the communication system has limited capacity. Three scenarios with same capacity constraint (10Mbps) and different wind information availability constraints (constrained range (500m), constrained update rate (0.3updates/min) and no constraints on wind map parameters) are observed in figures 4.5, 4.6 and 4.7 for the average of all wind scenarios. From these figures, one can observe that the optimal setting occurs when the capacity required for transmission is on the boundary of the feasible capacity. Thus, the fastest trajectory occurs when maximum information is available.

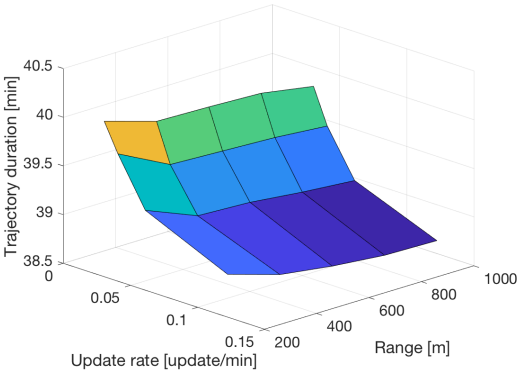


(a) packet error rate = 0.112

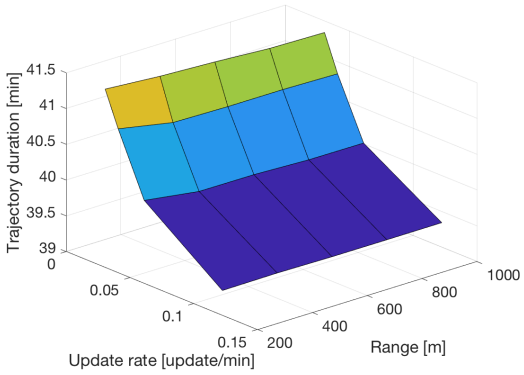


(b) packet error rate = 0.282

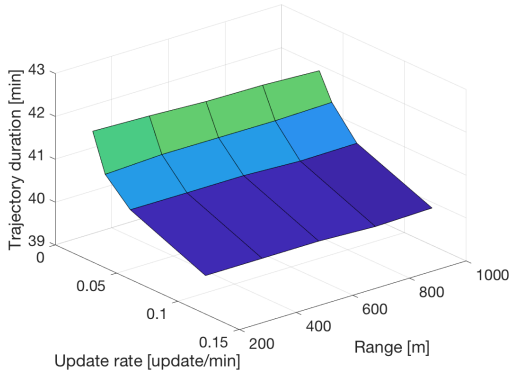


(c) packet error rate = 0.4457

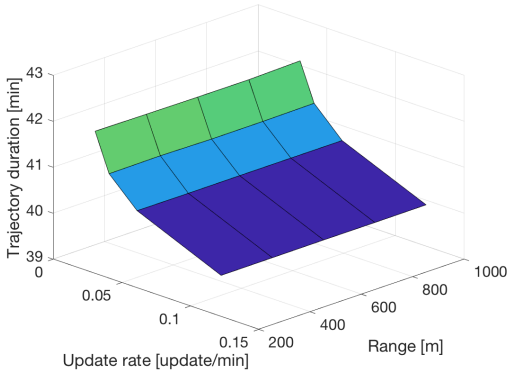


(d) packet error rate = 0.7051

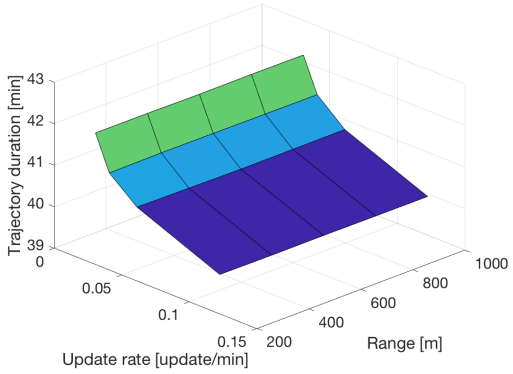


(e) packet error rate = 0.8408

Figure 4.3: Effect of communication imperfection in terms of packet error rate

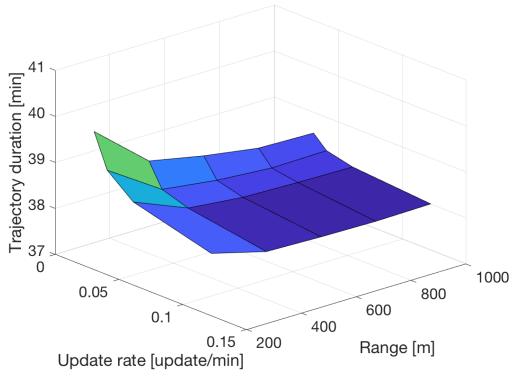


(a) bit error rate = 4.446e-5

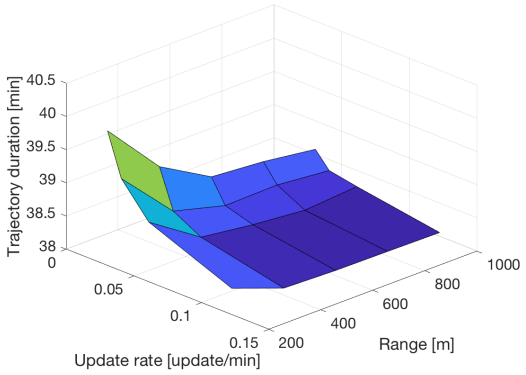


(b) bit error rate = 6.61e-4

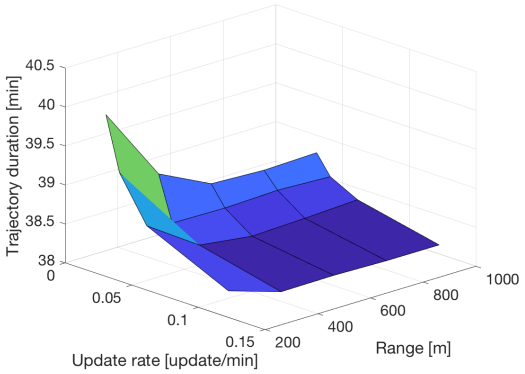


(c) bit error rate = 7.13e-3

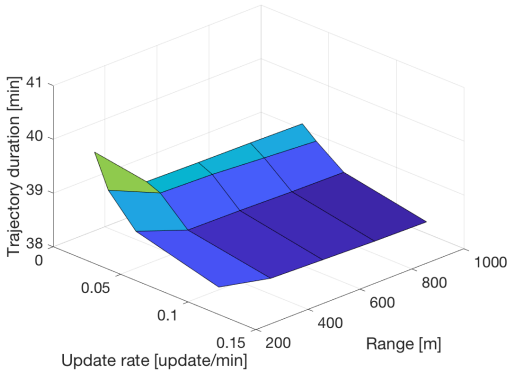


(d) bit error rate = 4.81e-2

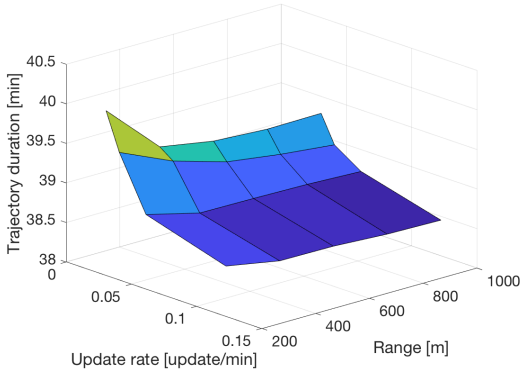


(e) bit error rate = 0.166

Figure 4.4: Effect of communication imperfection in terms of bit error rate

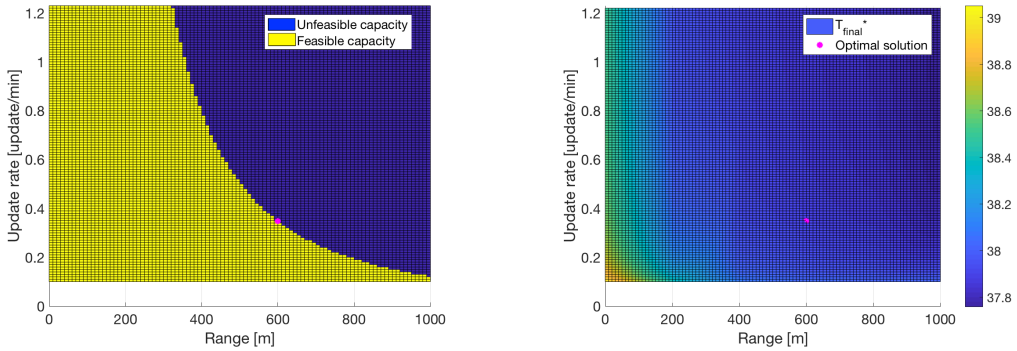


Figure 4.5: Effect of communication capacity constraint on the selection of wind map range and update rate

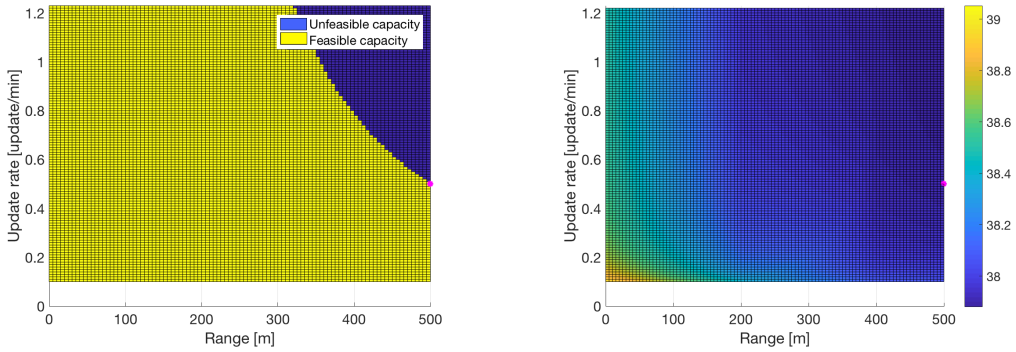


Figure 4.6: Effect of communication capacity and range constraint on the selection of wind map range and update rate

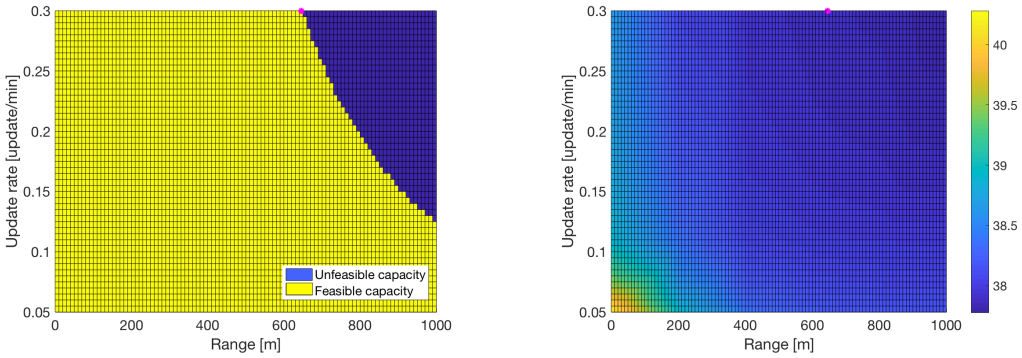


Figure 4.7: Effect of communication capacity and update rate constraint on the selection of wind map range and update rate

# CHAPTER 5

# IMPLEMENTATION OF A NAVIGATION SYSTEM FOR UAV

## 5.1 Introduction

When implementing a feedback system such as the path planning proposed in Chapter 3, it is vital to accurately measure/estimate the states of the system in which are used in the feedback loop. Therefore, this Chapter introduces a navigation system design and implementation.

A navigation system is usually comprised by sensors that can measure the states of a vehicle in motion. There are multiple forms of navigation which one can measure the position and orientation of UAVs. Often UAV navigation is performed using an on-board Inertial Measurement Unit (IMU). The IMU is capable of measuring linear and angular acceleration in 3-axis using accelerometers and gyroscopes. Based on its initial location and speed, the IMU can calculate the vehicle position and orientation. However, these sensors suffer error accumulation over time. Thus, GPS modules are usually combined to the IMU to compensate drift errors by fusing its data [39]. In addition to IMUs and GPS based navigation systems, studies in different directions have been conducted to enable navigation in GPS-denied environments by using alternative sensors such as laser scanners and cameras [39], [40]. However, for the purpose of this work, GPS-denied environments are not considered. A detailed description of the navigation system implementation is presented next.

## 5.2 Hardware and software description

The navigation system implementation described in this section is a combination of an IMU, GPS and barometer module. The sensors selected for this design were XSens MTI-3 (IMU), Adafruit Ultimate GPS module and the barometric sensor Adafruit BME280. The next three paragraphs give more details about each one of these sensors.

First, the XSens MTI-3, shown in Figure 5.1, is a device that outputs orientation, rate of turn, acceleration and magnetic field in all three axis. The selection of this device is mainly due to its compact size which is an important factor when designing UAV systems and its good accuracy [41]. Moreover, the device conveniently provides signal processing and conditioning on-board which facilitates its utilization. The XSens MTI-3 is compatible with multiple interfaces such as UART, I2C and SPI allowing flexibility in the design [41]. Some of the relevant sensor characteristics are provided in Table 5.1.

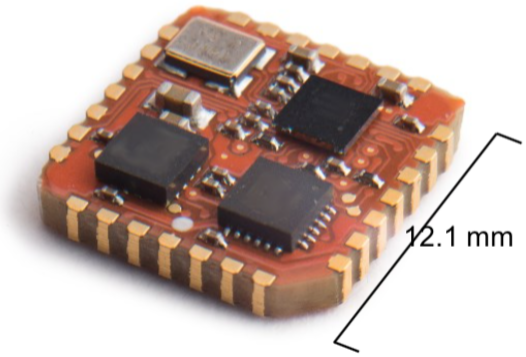


Figure 5.1: Inertial measurement unit: XSens MTI-3

Table 5.1: XSens MTI-3 important characteristics

| **Parameter name** | **Value** |
|---|---|
| Row accuracy | 1° |
| Pitch accuracy | 1° |
| Yaw accuracy | 2° |
| Gyroscope range | ±2000°/second |
| Gyroscope bias | 10°/hour |
| Accelerometer range | ±16g |
| Accelerometer bias | 0.1mg |
| Size | 12.1x12.1x2.55mm |
| Weight | 0.66 grams |
| Output data rate | up to 1kHz |
| Voltage | 3.3V |

Next, the Adafruit Ultimate GPS module, Figure 5.2, is a very popular GPS module among hobbyists and enthusiasts. This is an attractive reason due to the fact that lots of resources are available online which facilitates the development. In addition, this GPS module is a low cost device that has high sensitivity while consuming low power. Another important feature that contributes to the selection of this module is the fact that it can allow update rates up to 10Hz. Some of the relevant sensor characteristics are summarized in Table 5.2.

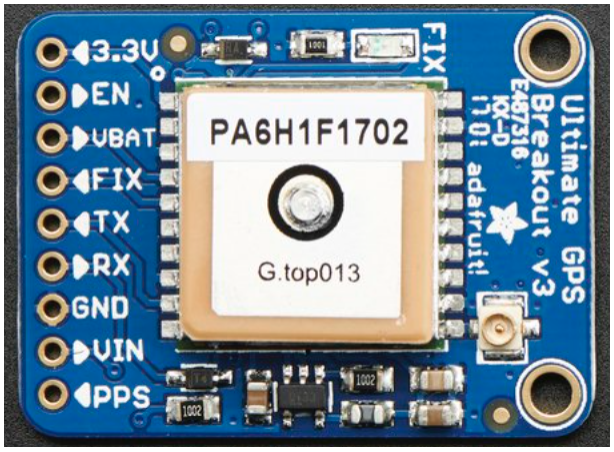


Figure 5.2: GPS module: Adafruit Ultimate GPS module

Table 5.2: Adafruit Ultimate GPS module important characteristics

| **Parameter name** | **Value** |
|---|---|
| Position accuracy | <3 m |
| Velocity accuracy | 0.1 m/s |
| Tracking sensitivity | -165 dBm |
| Size | 25.5x35x6.5mm |
| Weight | 8.5 grams |
| Output data rate | up to 10Hz |
| Voltage | 3-5.5V |
| Interface | UART |

Table 5.3: BME280 important characteristics

| **Parameter name** | **Value** |
|---|---|
| Altitude accuracy | ±1m |
| Size | 19x18x3mm |
| Weight | 1 gram |
| Voltage | 3-5.5V |
| Interface | I2C and SPI |

Finally, the barometric Adafruit BME280 sensor, Figure 5.3, is a simple sensor that measures the environmental air pressure. Given that there is a direct relationship between air pressure and altitude, the purpose of this sensor is to obtain the UAV altitude. From a pressure measurement, one can obtain the altitude as follows [42]:

$$h = 44330(1 - \frac{P_h}{P_0}^{0.1903}) \tag{5.1}$$

where, $h$ is the altitude in meters, $P_h$ and $P_0$ is the atmospheric pressure, in hPa, at altitude $h$ and at the ground level, respectively.

Moreover, this is a low cost and very accurate sensor. Similar to the GPS module, it is a very popular alternative among hobbyists which eases the development process due to extensive amount of information available online. Some of the relevant sensor characteristics are summarized in Table 5.3.

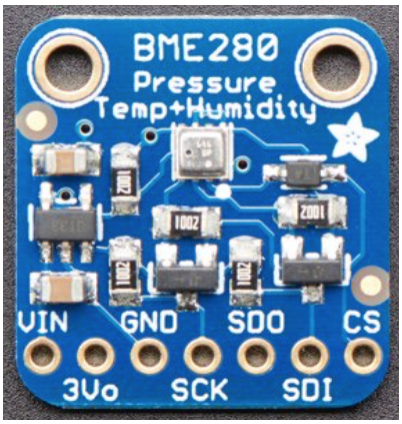


Figure 5.3: Barometer sensor: Adafruit BME280

Initially, the navigation system is prototyped using the Arduino MEGA2560 development board. Arduino is an user-friendly platform that allows rapid prototyping and offers a large support through its community. The MEGA2560 development board is based on the ATMEGA2560 chip that operates at 16MHz and has 16 analog inputs as well as 54 GPIO pins, which 16 of them can be configured as PWM pins. Moreover, it has multiple interfaces such as 4 UART, SPI and I2C pins that allows a vast number of sensor to be simultaneously connected to the board.

In this design, all sensors are interfaced with the microcontroller that is responsible for communicating to each sensor in order to acquire the measured data. The GPS and IMU modules communicate their measurements using UART and require that their messages are parsed in the microcontroller. On the other hand, the barometer communicates with the ATMEGA2560 microcontroller using I2C and no parsing is needed. In addition to the sensors, a microSD card slot is used in order to log all the data collected and it is interfaced using SPI.

The software implementation can be described as a three stage process. Initially, two UART ports are configured to communicate at 115200 baud/s and at 9600 baud/s

for the IMU and the GPS, respectively. In addition to the UART, I2C and SPI ports are configured. Next, once the communication between sensors and micrcontroller is arranged, the next stage consists in initializing the GPS, IMU as well as the barometer module. The GPS is set to communicate only the minimal required information (date, time, latitude, longitude, speed and fix) at a rate of 10Hz, while the IMU is set to transmit new data only when the microcontroller requests for it. The reference frame for the IMU measurements is East-North-Up (ENU) and the orientation data is originally given in quartenions but it is later converted to Euler angles. The last step in this stage is to allow the barometer to make a measurement in order to set the ground reference level, so the measured altitude is subject to the ground level as opposed to the sea level. Finally, the last stage comprises in entering measurement mode where the microcontroller will read the sensor data every 100ms and store it in the SD card memory. Figure 5.4 illustrates the stages of the software description.

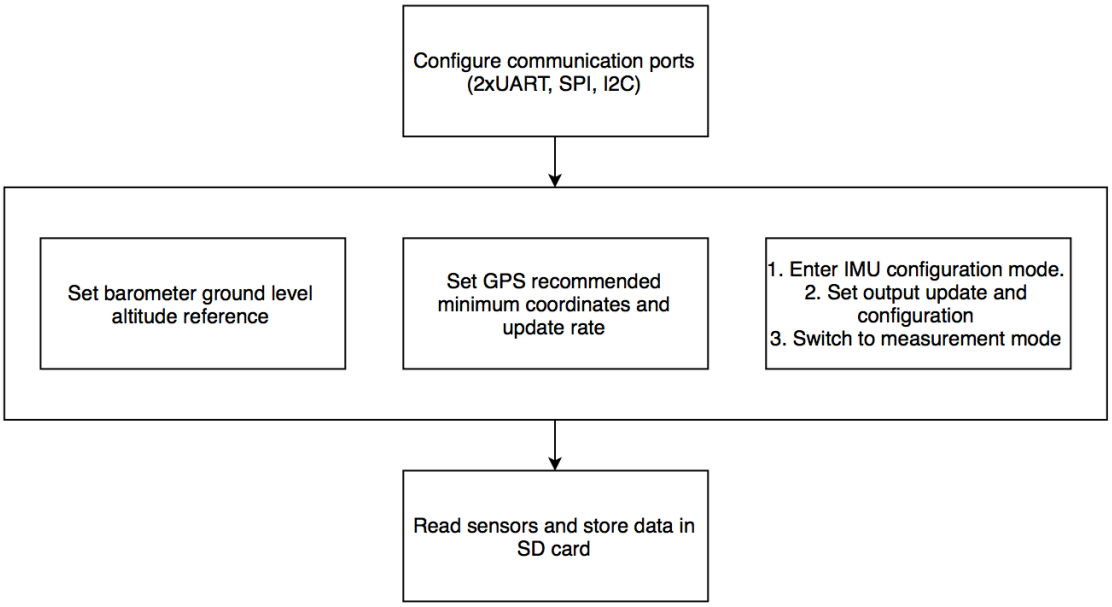


Figure 5.4: Stages of the software description

Once the implementation is successfully executed in the prototype, a final hardware design is implemented. In the hardware design, a compact printed circuit board (PCB) is created so it can be safely attached to the UAV. The custom board is based on the same ATMEGA2560 chip as the arduino board and since the navigation system requires mobility, the board is powered by a small 11.1V and 860mAh LiPo battery controlled by a power swicth. The battery output is converted by two voltage regulators to power the ATMEGA2560 chip with 5V and the sensors and microSD slot with 3.3V. Due the fact the microcontroller operates in 5V and the IMU and microSD card operates exclusively in 3.3V, a level shifter is required to step down the microcontroller output to match with the 3.3V peripheral input pins. Finally, the last addition to the custom board is a micro-USB port and an ATMEGA16u2 chip to interface the main microcontroller (ATMEGA2560 chip) to the computer where the software is developed. Thus, the software can be loaded in the final designed hardware. Figures 5.5, 5.6 and 5.7 show the final hardware designed.

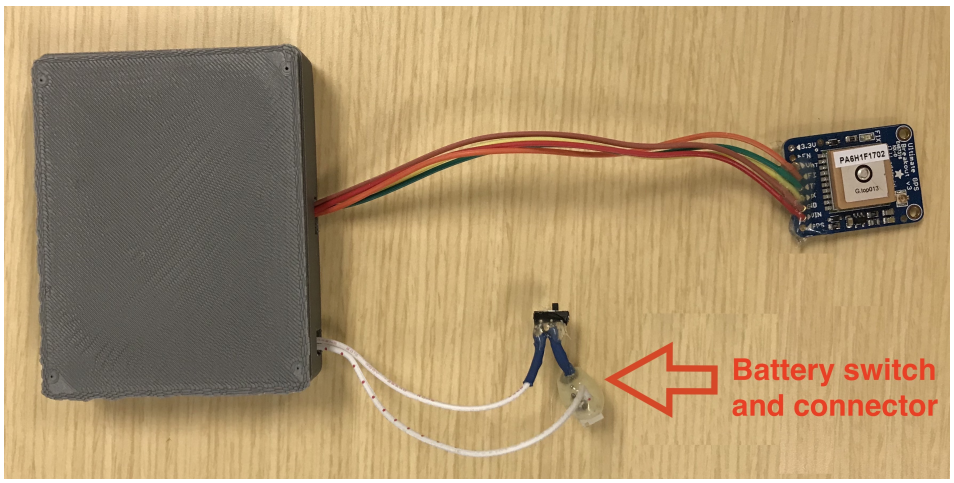


Figure 5.5: Final navigation system design enclosed in a case

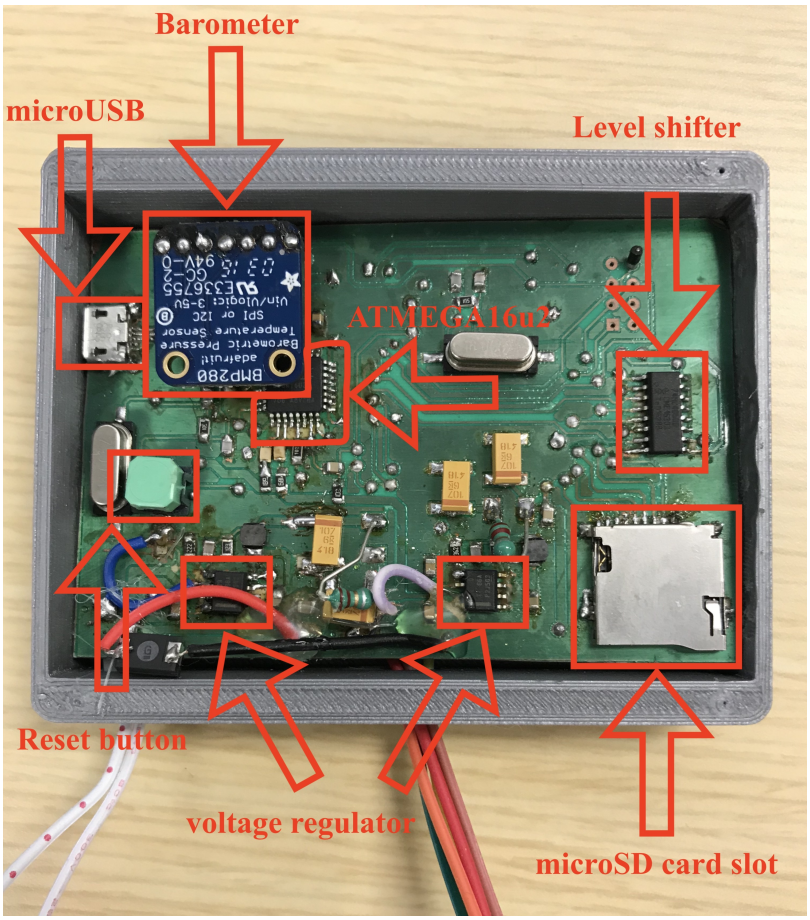


Figure 5.6: Top view of the final navigation system design

## 5.3 Results

This section focuses on the results obtained from the implementation of the navigation system described in Section 5.2. Multiple tests, including remote controlled fixed-wing aircraft and quadrotor flights, were executed to evaluate the performance of the navigation system. Figures 5.8 and 5.9 presents the results obtained when attaching the navigation system to a DJI Matrice 100 quadrotor. The purpose of this test was to validate the design by comparing the data collected using the custom system to the flight data stored by the Matrice 100 on its on-board computer. In this

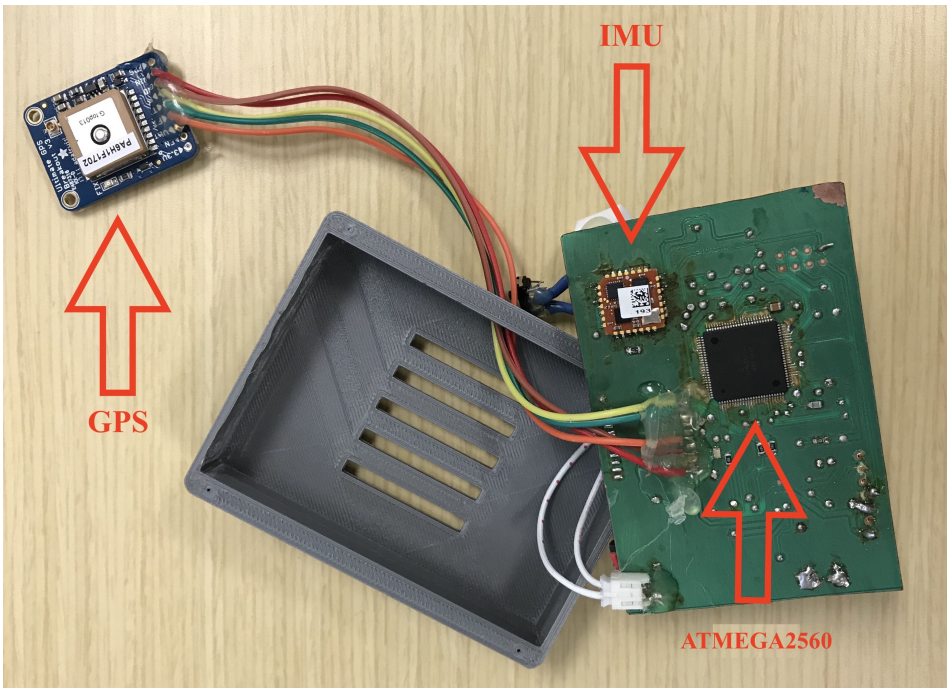


Figure 5.7: Bottom view of the final navigation system design

experiment, first the quadrotor moved in a rectangular shaped trajectory and later it performed rotation on its own vertical axis.

As can be observed, in both figures, the designed system presented a similar performance to the DJI on-board navigation system platform. Although the altitude and yaw measurement deviates from the reference, the overall behavior remains coherent. For the yaw measurement, which translates to the vehicle heading, this deviation is attributed to an existing offset of 75 degrees in the placement of the designed navigation system. In the case of the altitude, such discrepancy can be due to the fact that the Matrice 100 relies on GPS coordinates instead of using barometer.

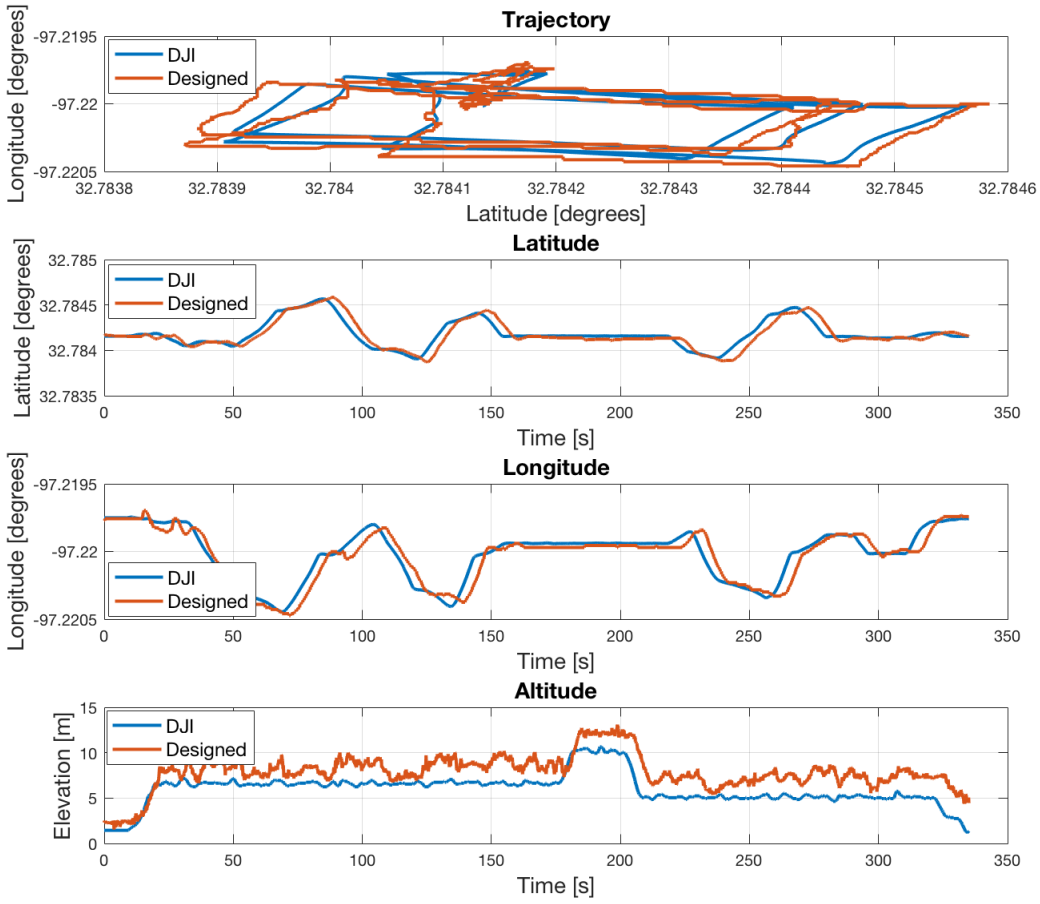


Figure 5.8: Comparison in terms of UAV position between the navigation system designed and the DJI Navigation system

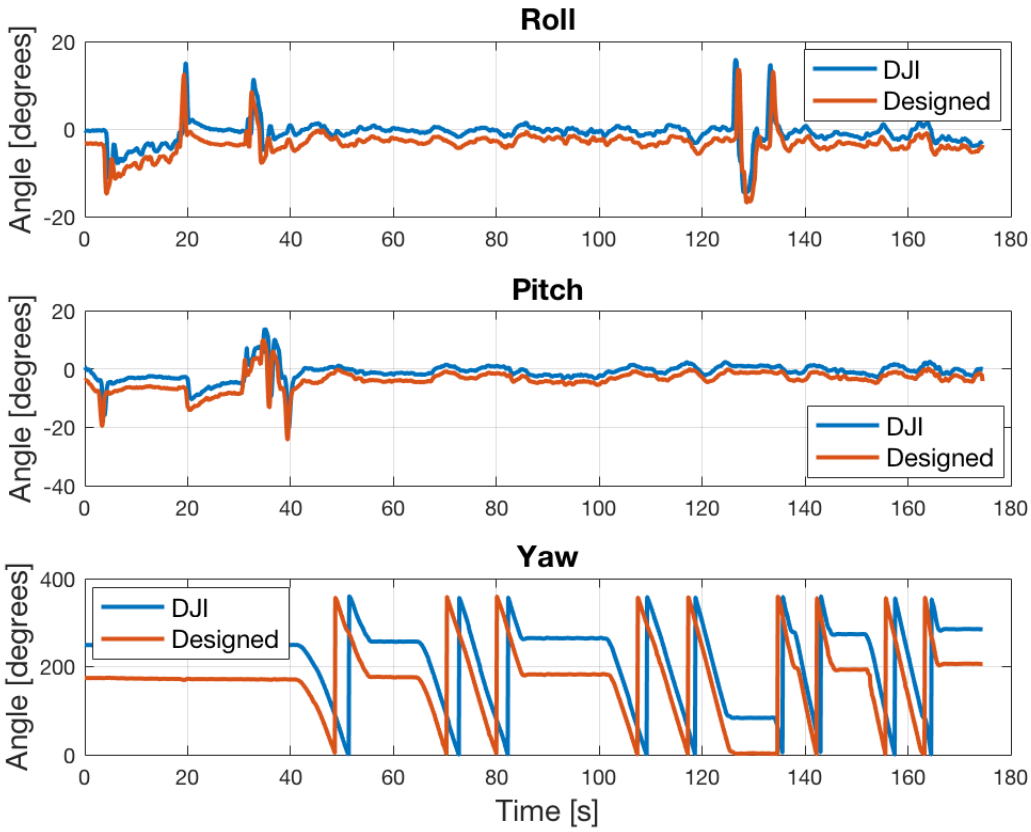


Figure 5.9: Comparison in terms of UAV orientation between the navigation system designed and the DJI Navigation system

# CHAPTER 6

# CONCLUSIONS

## 6.1 Conclusions

In this thesis, the problem of UAV on-board sensing and off-board sensing through wireless communication was investigated using UAV optimal path planning as a case study. A modeling framework including the communication channel, vehicle dynamics, and environmental impact was constructed along with a minimum-time optimal UAV path planning solution that utilizes on-board or off-board wind map information subject to communication constraints and spatiotemporal wind impact. It was found that both on-board sensing and off-board sensing, if properly used, can improve the path planning performance in terms of the trajectory duration. The duration decreases with the increase of the map update rate and map range for the on-board sensing and perfect communication cases. The performance of off-board sensing is significantly affected by the quality of the communication environment. With more limited channel performance measured by SNR and reflected in BER and PER, the trajectory duration of path planning is lengthened.

In addition, the path planing performance can be optimized by appropriately configuring the information update parameters (i.e., the update range and update rate) subject to the channel capacity and wind update information configuration constraints. The modeling and analytical framework developed in this work provides some initial insights on the trade-offs between on-board and off-board sensing.

Besides the theoretical the analysis described, an initial first step towards its practical implementation was executed. A navigation system for UAV was designed

and implemented. Tests were performed to validate the design using a navigation system built-in on a commercial quadrotor. The results obtained in the implementation behaved closely to the given reference demonstrating that the design can, in fact, be employed on real UAV platforms.

As an extension to this work, more comprehensive studies can be conducted on the optimal configurations of UAV on-board and off-board sensing and computation, UAV communication, and UAV information service provisions. Moreover, on the practical side, future work can complement the theoretical work developed in this thesis by implementing path planning on a real platform using off-board sensors.

REFERENCES


[1] M. Pinheiro, M. Liu, Y. Wan, and A. Dogan, "On the analysis of on-board sensing and off-board sensing through wireless communication for uav path planning in wind fields," *AIAA Scitech 2019 Forum*, January 2019.

[2] B. Wang, J. Xie, S. Li, Y. Wan, S. Fu, and K. Lu, "Enabling high-performance onboard computing with virtualization for unmanned aerial systems," in *IEEE International Conference on Unmanned Aircraft Systems (ICUAS)*, 2018.

[3] J. Chen, J. Xie, Y. Gu, S. Li, S. Fu, Y. Wan, and K. Lu, "Long-range and broadband aerial communication using directional antennas (acda): design and implementation," *IEEE Transactions on Vehicular Technology*, vol. 66, no. 12, pp. 10 793–10 805, 2017.

[4] V. Roberge, M. Tarbouchi, and G. Labonté, "Comparison of parallel genetic algorithm and particle swarm optimization for real-time uav path planning," *IEEE Transactions on Industrial Informatics*, vol. 9, no. 1, pp. 132–141, 2013.

[5] F. Wantuch, Z. Bottyán, Z. Tuba, and K. Hadobács, "Statistical methods and weather based decision making in meteorological support for unmanned aerial vehicles (uavs)," in *IEEE International Conference on Unmanned Aircraft Systems (ICUAS)*, 2013.

[6] J.-W. Kampoon, "Wind field estimation and its utilization in trajectory and input prediction," *PhD thesis, University of Texas at Arlington*, 2014.

[7] M. B. Rhudy, T. Larrabee, H. Chao, Y. Gu, and M. Napolitano, "Uav attitude, heading, and wind estimation using gps/ins and an air data system," in *AIAA Guidance, Navigation, and Control (GNC) Conference*, 2013.

[8] R. V. I. Rachelle L. McNeely and P. R. Chandler, "Tour planning for an unmanned air vehicle under wind conditions," *Journal of Guidance, Control, and Dynamics*, vol. 30, no. 5, pp. 1299–1306, 2007.

[9] P. Marinova, "Determination of an area avoidance wind optimal trajectory by the methods of optimal control," *Master thesis, University of Hamburg*, 2012.

[10] J. Guerrero and Y. Bestaoui, "Uav path planning for structure inspection in windy environments," *Journal of Intelligent and Robotic Systems*, vol. 69, pp. 297–311, 2013.

[11] D. W. Casbeer, R. W. Beard, T. W. McLain, S.-M. Li, and R. K. Mehra, "Forest fire monitoring with multiple small uavs," in *Proceedings of the American Control Conference*, 2005.

[12] B. Girardet, L. Lapasset, D. Delahaye, and C. Rabut, "Wind-optimal path planning: Application to aircraft trajectories," in *2014 13th International Conference on Control Automation Robotics Vision (ICARCV)*, Dec 2014, pp. 1403–1408.

[13] W. Al-Sabban, L. Gonzalez, and R. Smith, "Wind-energy based path planning for electric unmanned aerial vehicles using markov decision processes," 01 2013.

[14] C. He, Y. Wan, and F. L. Lewis, "On the identifiability of the influence model for stochastic spatiotemporal spread processes," *Submitted to 2019 American Control Conference (ACC)*, 2018.

[15] J. Xie, Y. Wan, Y. Zhou, S.-L. Tien, E. P. Vargo, C. Taylor, and C. Wanke, "Distance measure to cluster spatiotemporal scenarios for strategic air traffic management," *Journal of Aerospace Information Systems*, vol. 12, no. 8, pp. 545–563, 2015.

[16] Y. Qu, Z. Xing, Y. Zhang, and Z. Yu, "Real-time wind vector estimation for a micro uav," in *Proceedings of International Conference on Unmanned Aircraft Systems (ICUAS)*, 2017.

[17] P. P. Neumann, "Real-time wind estimation on a micro unmanned aerial vehicle using its inertial measurement unit," *Sensors and Actuators A: Physical*, vol. 235, pp. 300–310, nov 2015.

[18] D. Hollenbeck, G. Nunez, L. E. Christensen, and Y. Chen, "Wind measurement and estimation with small unmanned aerial systems (suas) using on-board mini ultrasonic anemometers," *2018 International Conference on Unmanned Aircraft Systems (ICUAS)*, pp. 285–292, 2018.

[19] A. Al-Hourani, S. Kandeepan, and S. Lardner, "Optimal lap altitude for maximum coverage," *IEEE Wireless Communications Letters*, vol. 3, no. 6, pp. 569–572, 2014.

[20] D. Pareit, V. Petrov, B. Lannoo, E. Tanghe, W. Joseph, I. Moerman, P. Demeester, and L. Martens, "A throughput analysis at the mac layer of mobile wimax," in *Proceedings of IEEE Wireless Communication and Networking Conference*, 2010.

[21] Y. Zeng, R. Zhang, and T. Lim, "Wireless communications with unmanned aerial vehicles: Opportunities and challenges," *IEEE Communications Magazine*, vol. 54, 2016.

[22] K. Gomez, T. Rasheed, L. Reynaud, and S. Kandeepan, "On the performance of aerial lte base-stations for public safety and emergency recovery," pp. 1391–1396, Dec 2013.

[23] Y. Wan, K. Namuduri, Y. Zhou, and S. Fu, "A smooth-turn mobility model for airborne networks," *IEEE Transactions on Vehicular Technology*, vol. 62, no. 7, pp. 3359–3370, 2013.

[24] Y. Gu, M. Zhou, S. Fu, and Y. Wan, "Airborne wifi networks through directional antennae: An experimental study," in *Wireless Communications and Networking Conference (WCNC), 2015 IEEE*. IEEE, 2015, pp. 1314–1319.

[25] J. Xie, Y. Wan, J. H. Kim, S. Fu, and K. Namuduri, "A survey and analysis of mobility models for airborne networks," *IEEE Communications Surveys & Tutorials*, vol. 16, no. 3, pp. 1221–1238, 2014.

[26] C. Dixon and E. W. Frew, "Optimizing cascaded chains of unmanned aircraft acting as communication relays," *IEEE Journal on Selected Areas in Communications*, vol. 30, no. 5, pp. 883–898, 2012.

[27] I. Bor-Yaliniz, A. El-Keyi, and H. Yanikomeroglu, "Efficient 3-d placement of an aerial base station in next generation cellular networks," 02 2016.

[28] U. Challita and W. Saad, "Network formation in the sky: Unmanned aerial vehicles for multi-hop wireless backhauling," pp. 1–6, Dec 2017.

[29] E. Kalantari, H. Yanikomeroglu, and A. Yongacoglu, "On the number and 3d placement of drone base stations in wireless cellular networks," pp. 1–6, 09 2016.

[30] S. Jia and L. Zhang, "Modelling unmanned aerial vehicles base station in ground-to-air cooperative networks," *IET Communications*, vol. 11, no. 8, pp. 1187–1194, 2017.

[31] ITU-R, "Propagation data and prediction methods required for the design of terrestrial broadband radio access systems operating in a frequency range from 3 to 60 ghz," International Telecommunication Union Radiocommunication Sector (ITU-R), Tech. Rep. Recommendation ITU-R P.1410- 5, February 2012.

[32] A. Goldsmith, *Wireless Communication System*. Stanford University: Cambridge University Press., 2005.

[33] A. Pokkunuru, Q. Zhang, and P. Wang, "Capacity analysis of aerial small cells," in *2017 IEEE International Conference on Communications (ICC)*, May 2017, pp. 1–7.

[34] J. Holis and P. Pechac, "Elevation dependent shadowing model for mobile communications via high altitude platforms in built-up areas," *IEEE Transactions on Antennas and Propagation*, vol. 56, no. 4, pp. 1078–1084, April 2008.

[35] M. S. John G. Proakis, *Digital Communications*, 5th ed. New York: McGraw-Hill, 2008.

[36] S. C. Bretmersky, W. D. Bishop, J. Dailey, and C. T. Chevalier, "Communications technology assessment for the unmanned aircraft system (uas) control and non-payload communications (cnpc)," NASA Glenn Research Center, Tech. Rep., June 2014. [Online]. Available: https://ntrs.nasa.gov/archive/nasa/casi.ntrs.nasa.gov/20140010476.pdf

[37] "Ieee standard for air interface for broadband wireless access systems," *IEEE Std 802.16-2012 (Revision of IEEE Std 802.16-2009)*, pp. 1–2542, 2012.

[38] J. P. How, "Principles of optimal control, (mit opencourseware)," in *(Accessed March 1, 2018) License: Creative Commons BY-NC-SA*, 2008. [Online]. Available: https://ocw.mit.edu/courses/aeronautics-and-astronautics/16-323-principles-of-optimal-control-spring-2008/lecture-notes/lec7.pdf

[39] G. Balamurugan, V. Jayaraman, and D. V. Naidu, "Survey on uav navigation in gps denied environments," 10 2016, pp. 198–204.

[40] A. Bachrach, A. de Winter, R. He, G. Hemann, S. Prentice, and N. Roy, "Range - robust autonomous navigation in gps-denied environments," in *2010 IEEE International Conference on Robotics and Automation*, May 2010, pp. 1096–1097.

[41] *Data sheet MTi 1-series*, XSens, 12 2016, rev. D.

[42] *A Quick Derivation relating altitude to air pressure*, Portland State Aerospace Society, 12 2004.

## BIOGRAPHICAL STATEMENT

Murilo A. Pinheiro was born in Campinas, Brazil, in 1990. In June of 2016, he received his bachalor degree in Electrical Engineering with emphasis in electronics from University of Sao Paulo. Two months later, he joined The University of Texas at Arlington for his master of science degree and specialization in control systems. In 2017, Murilo joined the Dynamic Network and Control lab under Dr. Wan supervision to pursue further research in UAV applications and unmanned vehicle systems. He is fascinated and inspired by natures perfection and he believes that mimicking nature can bring much advancements to the society. His research interests include autonomous vehicle systems, robotics and multi-agent systems. He worked as a teaching and research assistant for The University of Texas at Arlington for Dr. Wan.